Ordered and chaotic dynamics of collective variables in a butane molecule

Anna Battisti,* Rocco G. Lalopa, and Alexander Tenenbaum†
Physics Department, Sapienza University, Piazzale Aldo Moro 2, 00185 Rome, Italy

Maira D'Alessandro
Chemistry Department, Sapienza University, Piazzale Aldo Moro 2, 00185 Rome, Italy

(Received 13 July 2008; revised manuscript received 23 February 2009; published 6 April 2009)

We have simulated the dynamics of a butane molecule and computed the time evolution of two sets of collective variables: (a) internal variables (stretchings, bendings, and dihedral angle) and (b) variables derived from a principal component analysis (PCA). We have characterized each collective variable by a coherence time, the time needed to develop its chaotic behavior. The coherence times diminish significantly when the temperature is raised into and above the range where conformational transitions of the dihedral angle set in. Below this transition region the coherence times of some variables reach hundreds of picoseconds (principal components) or even nanoseconds (internal variables); moreover, there are large differences among variables, as their coherence time can be much larger or much smaller than the Lyapunov time of the whole molecule. This result reflects the prediction of Nekhoroshev's theorem. Crossing the transition region, the coherence times of both sets of variables drop to few picoseconds, and the differences among variables diminish. Still, the coordinates and velocities characterized by the largest fluctuations in the PCA appear to be also the most coherent ones, below and above the transition region.

DOI: 10.1103/PhysRevE.79.046206 PACS number(s): 05.45.Pq, 33.15.−e

I. INTRODUCTION

The very first study of a condensed-matter system that showed the (unexpected) existence of an ordered dynamical regime is the well-known computer simulation by Fermi, Pasta, and Ulam (FPU) back in 1953 [1]. Since then, many papers have been published in this field, dealing with the chaotic behavior of model or realistic systems. Ordered behavior has been found mostly in systems with few degrees of freedom (DOFs), while larger systems have often been found to be chaotic. The theoretical explanation of the appearance of ordered motions in nonlinear systems begun at the same time—but independently—as the FPU experiment and is known as the Kolmogorov, Arnold, and Moser (KAM) theorem [2]. This theorem explained why a nonlinear system may be endowed with regular motions, provided the nonlinearity is not too large; this property was attributed to the system as a whole. A later theorem by Nekhoroshev [3] foresaw the possibility that within a chaotic system different DOFs may exhibit their chaotic behavior on very different time scales. A computer simulation that yielded evidence of the type of dynamics foreseen by Nekhoroshev [3] was done on a lattice of particles interacting via a Lennard-Jones potential [4,5]; there, at low energy, the dynamics showed a mixed pattern, as different normal modes became chaotic over a time that could be very different (by several orders of magnitude) for normal modes of different frequency. This phenomenology stresses the necessity—when analyzing the dynamics of a nonlinear system—of applying adequate diagnostic tools to study the behavior of individual DOFs besides the tools usually implemented to study the behavior of the system as a whole (Lyapunov spectrum, spectral entropy, and stochastic threshold). In Sec. II we review the development of some diagnostic tools already used in studying individual DOFs in condensed-matter systems and explain the choice made for the present study. In Sec. III we describe how to measure a coherence time for each DOF. In Sec. IV we describe the model of butane used in our computer experiment. In Sec. V we perform a standard analysis of the system by computing the Lyapunov spectrum. In Sec. VI we apply our diagnostic tools to the dynamical behavior of the internal variables of the butane molecule. In Sec. VII we discuss a different set of collective variables, those derived from a principal component analysis (PCA) of the system's trajectory in the phase space, and in Sec. VIII we analyze the coherence of the variables defined in the PCA. In Sec. IX we discuss our results and compare them with previous work done on the same system. In Sec. X we draw the conclusions.

II. COHERENCE OF INDIVIDUAL DEGREES OF FREEDOM

A chaotic system is usually characterized by a fast exponential rate of divergence of trajectories beginning at near points in the phase space. We call coherence the inverse property of chaoticity, namely, a slow divergence of near trajectories. In this section we analyze this property.

Let us briefly recall the theory of the Lyapunov exponents. Let $\mathbb{R}^m$ be a differentiable, m-dimensional, compact, and connected Riemannian manifold of class C^2. If $\mathbf{x} \in \mathbb{R}^m$, we denote by $T\mathbb{R}^m$ the tangent space to $\mathbb{R}^m$ in $\mathbf{x}$. Let $\Phi^t: \mathbb{R}^m \to \mathbb{R}^m$ be a flow generated by the set of differential equations $\dot{\mathbf{x}} = \mathbf{f}(\mathbf{x})$; the tangent mapping of $T\mathbb{R}^m_{\mathbf{x}}$ onto $T\mathbb{R}^m_{\Phi^t_{\mathbf{x}}}$, induced by the diffeomorfism Φ^t, will be denoted by $d\Phi^t_{\mathbf{x}}$.

*Now at FBK-Center for Materials and Microsystems, Via Sommarive 18, 38050 Povo (Trento), Italy.
†Author to whom correspondence should be addressed; alexander.tenenbaum@roma1.infn.it

Oseledec [6] (see also Refs. [7] and [8]) proved that an orthonormal base $\{\mathbf{e}_i\}$ exists in $T\mathbb{R}^m_{\mathbf{x}}$, such that

$$\lim_{t\to\infty}\frac{1}{t}\ln\|d\Phi^t_{\mathbf{x}}(\mathbf{e}_i)\| = \lambda(\mathbf{x},\mathbf{e}_i) = \lambda_i(\mathbf{x}).$$

The numbers $\lambda_i(\mathbf{x})$ are called the Lyapunov characteristic exponents and give a measure of the rate of divergence in the phase space of initially nearby trajectories. The $\lambda_i(\mathbf{x})$ are not necessarily distinct; we denote by $\{\nu_j\}_{1\le j\le s}$ the distinct values taken by $\{\lambda_i(\mathbf{x})\}_{1\le i\le m}$ and by $k_j(\mathbf{x})$ the multiplicity of $\nu_j(\mathbf{x})$. We also let $\nu_i \ge \nu_j$ if $i \le j$. Then a theorem [7] states that there exist linear subspaces $H_1,\ldots,H_s$, $s=s(\mathbf{x})$ such that $T\mathbb{R}^m_{\mathbf{x}} = H_1 \oplus \cdots \oplus H_s$ and $\dim H_j = k_j(\mathbf{x})$. If $\mathbf{e}\neq 0$, and $\mathbf{e}\in H_j \oplus H_{j+1}\oplus\cdots\oplus H_s$ but $\mathbf{e}\notin H_{j+1}\oplus H_{j+2}\oplus\cdots\oplus H_s$, then $\lambda(\mathbf{x},\mathbf{e}) = \nu_j(\mathbf{x})$. If the system is ergodic, the whole set $\{\lambda_i\}$ is independent of $\mathbf{x}$ (almost everywhere). In this case, choosing a vector $\mathbf{e}$ at random in $T\mathbb{R}^m_{\mathbf{x}}$ one may expect to find $\lambda(\mathbf{x},\mathbf{e}) = \lambda_1$. From now on the set $\{\nu_j\}$ will be denoted by $\{\lambda_j\}$.

The first ways to compute the Lyapunov exponents were to follow the dynamics of two initially nearby trajectories and to study the evolution of their distance; a rescaling mechanism was then added to avoid a possible exponential overflow of that distance [9]. Later a second way was developed, in which the dynamics in the tangent space of the phase space was computed by linearizing the equations of motion. If $\dot{\mathbf{x}}=\mathbf{f}(\mathbf{x})$, $\mathbf{x}\in\mathbb{R}^m$, the linear evolution of a tangent vector $\mathbf{w}\in T\mathbb{R}^m_{\mathbf{x}}$, the tangent space in $\mathbf{x}$, is given by

$$\dot{w}_i(t) = \sum_{k=1}^{m}\frac{\partial f_i}{\partial x_k}w_k(t), \quad i=1,m.$$

From the theorems mentioned before, there is a base $\{\mathbf{e}_i\}$ in $T\mathbb{R}^m_{\mathbf{x}(0)}$, such that for almost all initial conditions the long time evolution of $\mathbf{w}$ is given by a superposition of vectors, the coefficients of which are exponentials of the Lyapunov exponents λ_j,

$$\mathbf{w}(t) = \sum_{j=1}^{s}\mathbf{a}_j(t)e^{\lambda_j t},$$

where $s\le m$, $\mathbf{a}_j \equiv \Sigma_i|\mathbf{w}(0)|\mathbf{c}_i(t)\mathbf{e}_i$, and this sum is done over all $\mathbf{e}_i$ characterized by the same expansion rate λ_j. The matrices $\mathbf{c}_i(t)$ entail a possible time dependence weaker than the exponential one and the rotation of $\{\mathbf{e}_i\}$ generated by the flow of the dynamics.

Let the phase space be decomposed into the sum of n subspaces, $S_1, S_2, \ldots, S_n (n\le m)$, which are physically interesting for the study of the system (they can also be single DOFs). This phase space decomposition will induce an analogous decomposition of the tangent space in n subspaces $TS_1, TS_2, \cdots, TS_n$.

A set of *coherence angles* (CAs) α_l, $l=1,\ldots,n$ can be defined through

$$\cos^2\alpha_l = \lim_{t\to\infty}\frac{1}{t}\int_0^t \frac{|\mathbf{w}^{(l)}(t')|^2}{|\mathbf{w}(t')|^2}dt',$$

where $\mathbf{w}^{(l)}(t)$ is the projection of $\mathbf{w}(t)$ on TS_l. Asymptotically $\mathbf{w}(t)\to\mathbf{a}_1(t)\exp(\lambda_1 t)$ and $\mathbf{w}^{(l)}(t)\to\mathbf{a}_1^{(l)}(t)\exp(\lambda_1 t)$, where $\mathbf{a}_1^{(l)}$ is the projection of $\mathbf{a}_1$ on TS_l [10]. So we have that

$$\cos^2\alpha_l = \lim_{t\to\infty}\frac{1}{t}\int_0^t \frac{|\mathbf{a}_1^{(l)}(t')|^2}{|\mathbf{a}_1(t')|^2}dt',$$

and each α_l represents an average angle between the subspace TS_l and the maximum expansion subspace. The TS_l are a fixed characteristic of the system; on the other hand, the maximum expansion subspace depends only on the phase space representative point and oscillates during the time evolution around an average direction in $T\mathbb{R}^m_{\mathbf{x}(t)}$. It follows that the CAs have a weak dependence on the initial conditions in the tangent space and in the phase space.

The coherence angles provide a mean to single out those DOFs which are endowed with a degree of coherence different from that of the whole system. DOFs characterized by a high value of the coherence angle have a high degree of coherence and may therefore require very long times to reach equilibrium.

The CAs measure the angular distance between the TS_l associated with the various DOFs and the maximum expansion subspace H_1 corresponding to λ_1 and are well defined asymptotically. But in the short and medium times, the evolution of a tangent vector and of its projections on the TS_l subspaces depends on its position relative to all the subspaces H_j, corresponding to the whole set of different Lyapunov exponents. In condensed-matter systems the Lyapunov spectrum is smooth: the exponents following the first have values slowly decreasing from the maximum one. As the chaoticity of a DOF increases with the angular proximity in the tangent space of its associated TS_l to a rapidly expanding subspace, it is clear that one should also consider the subspaces H_j corresponding to expansion coefficients just below λ_1. More generally, one can expect the short and medium time behaviors of a DOF to depend on the angular distance of its associated TS_l from all s subspaces H_j corresponding to Lyapunov exponents, whether expanding or contracting.

Let us call $\{\alpha_{jl}\}$ these *generalized coherence angles*; they completely characterize the time evolution of all subspaces of the tangent space [11,12]. The tangent space seems to be structured in such a way that the angles between a generic tangent vector and the most expanding directions have similar values, and the same holds for the most contracting ones. By this we mean that the projection of a tangent vector on a subspace characterized by a given Lyapunov exponent turns out to be similar in magnitude to the projection on another subspace characterized by a Lyapunov exponent similar to the previous one [13]. Therefore, the chaoticity of a DOF is determined mainly by the set of angles; its associated TS_l makes with the subspaces labeled by the Lyapunov exponents closely following the first (maximum) one.

In principle, all generalized coherence angles are necessary to completely define a degree of coherence for all DOFs. However, the computation of $n\times m$ terms can become a heavy task for large systems. In addition to the computational burden, using the whole set $\{\alpha_{jl}\}$ would make it impossible to take advantage of the synoptic view provided by a single coherence spectrum, like the one entailing only the

angles with the most expanding subspace, where the coherence of each DOF is measured by a single number [10].

There is also problem in measuring precisely the degree of coherence of the most ordered DOFs when the number n of physically interesting DOFs becomes very large. One can define a coherence angle α averaged over all DOFs of the system, for which the relation $\cos\alpha=1/\sqrt{n}$ holds [10]. The most coherent DOFs are characterized by angles confined in a range between α and $\pi/2$, which becomes narrow when n becomes large; they are thus difficult to distinguish, even if they are endowed with very different degrees of coherence. Moreover, it could be difficult to compare coherence properties of systems with different numbers of DOFs, as α depends on n. In the following we show how to circumvent these problems.

III. COHERENCE TIMES

We have looked for a new tool independent of n, physically meaningful and entailing all the relevant information on the short and medium time behaviors of the DOFs. This procedure allows the coherence of each DOF to be measured by a single number, the coherence time. The natural starting point is given by the effective expansion coefficients $\lambda^{(l)}(t)$; they synthesize the effect of all expanding and contracting directions in the phase space on the time evolution of each DOF. We define the following time-dependent quantities:

$$\lambda_1(t)=\frac{1}{t}\ln\frac{|\mathbf{w}(t)|}{|\mathbf{w}(0)|},$$

and a partial Lyapunov exponent (PLE) for each single DOF [14],

$$\lambda^{(l)}(t)=\frac{1}{t}\ln\frac{|\mathbf{w}^{(l)}(t)|}{|\mathbf{w}^{(l)}(0)|}.$$

$\lambda^{(l)}(t)$ characterizes the rate of divergence of the lth DOF for nearby trajectories in the same way as $\lambda_1(t)$ does for the total divergence of the trajectories. From the theorems quoted in Sec. II, we can conclude that $\lim_{t\to\infty}\lambda^{(l)}(t)=\lim_{t\to\infty}\lambda_1(t)=\lambda_1\ \forall\, l$.

$\lambda_1(t)$ and $\lambda^{(l)}(t)$ are computed as time averages over short segments of the trajectory of length ζ,

$$\lambda_1(t)=\frac{1}{N}\sum_{r=1}^{N}\frac{1}{\zeta}\ln\frac{|\mathbf{w}(r\zeta)|}{|\mathbf{w}[(r-1)\zeta]|}$$

and

$$\lambda^{(l)}(t)=\frac{1}{N}\sum_{r=1}^{N}\frac{1}{\zeta}\ln\frac{|\mathbf{w}^{(l)}(r\zeta)|}{|\mathbf{w}^{(l)}[(r-1)\zeta]|},$$

where $t=N\zeta$. Let $t_r=r\zeta$; we may interpret

$$\tilde{\lambda}_1(t_r)=\frac{1}{\zeta}\ln\frac{|\mathbf{w}(r\zeta)|}{|\mathbf{w}[(r-1)\zeta]|}$$

and

$$\tilde{\lambda}^{(l)}(t_r)=\frac{1}{\zeta}\ln\frac{|\mathbf{w}^{(l)}(r\zeta)|}{|\mathbf{w}^{(l)}[(r-1)\zeta]|}$$

as the segment-dependent expansion rates of the whole system and of the lth DOF, respectively. In the short and medium times, when the vector representing in the tangent space the distance between near trajectories has just begun reorienting in the direction of maximum expansion, $\tilde{\lambda}^{(l)}(t_r)$ may differ substantially from $\tilde{\lambda}_1(t_r)$. During this time, DOFs characterized by a higher (lower) coherence than the whole system should produce $\tilde{\lambda}^{(l)}(t_r)$ smaller (larger) than $\tilde{\lambda}_1(t_r)$ on most segments. $\lambda^{(l)}(t)$ may thus differ substantially from $\lambda_1(t)$ on the short and medium times. The value $\lambda^{(l)}(t)$ gives information about the accumulated exponential rate of expansion; therefore, it may be—before the relaxation to λ_1—lower or higher than $\lambda_1(t)$. This difference and the time needed to reach the regime where $\lambda^{(l)}(t)\cong\lambda_1$ characterize each DOF.

$\lambda^{(l)}(t)\to\lambda_1$ almost anywhere in the tangent space, but the time $\hat{t}$ after which $\lambda^{(l)}\cong\lambda_1$, that is the time each DOF needs to reach the asymptotic expansion rate of the whole system, is difficult to determine, as there is not a neat transition to the asymptotic behavior [14]. By observing the behavior of $\lambda^{(l)}(t)$ vs t, one can understand the approach to relaxation of each DOF. We gave in Figs. 1 and 2 of Ref. [14] the results obtained at low and high energies for the normal modes of a two-dimensional (2D) square lattice of particles interacting via a Lennard-Jones potential. We reported $t\lambda^{(l)}(t)$ vs t, so that the slope of the curves gave $\lambda^{(l)}(t)$. At the highest energy, where the whole system is in the chaotic regime, all subspaces behave alike, and the curves corresponding to $\lambda^{(l)}(t)$ are similar and near to the global one relative to $\lambda_1(t)$, an almost straight line with slope λ_1; still, a small but definite distance among lines referring to different DOFs is evident. At the lowest energy this distance is more visible, and one can observe a differentiated behavior of the DOFs, typical for a partially ordered dynamics.

This distance is the result of the combined effect of the accumulated difference between each $\lambda^{(l)}(t)$ and $\lambda_1(t)$ and of the time $\hat{t}_l$ needed to relax; roughly speaking, $\tilde{\lambda}^{(l)}(t)$ evolves to $\tilde{\lambda}_1$ up to $\hat{t}_l$, while $\tilde{\lambda}^{(l)}(t)\approx\tilde{\lambda}_1$ when $t>\hat{t}_l$. The distance is easily computable, and the precision of this measure increases with increasing averaging times because the distance between the lines $t\lambda^{(l)}(t)$ and $t\lambda_1(t)$ oscillates around its average value when $t\to\infty$ [14].

A hierarchy of coherence among the DOFs can be established by computing, during the dynamics, the vertical distances between each line $t\lambda^{(l)}(t)$ and the line $t\lambda_1(t)$ and averaging on time. The averaged horizontal distances, which we call *time shifts*, are then obtained dividing the vertical distances by the average common slope λ_1,

$$\tau^{(l)} = \frac{1}{\lambda_1}\lim_{t\to\infty}\frac{1}{t}\int_0^t t'[\lambda_1(t') - \lambda^{(l)}(t')]dt'$$
$$= \frac{1}{\lambda_1}\lim_{t\to\infty}\frac{1}{t}\int_0^t \left(\ln\frac{|\mathbf{w}(t')|}{|\mathbf{w}(0)|} - \ln\frac{|\mathbf{w}^{(l)}(t')|}{|\mathbf{w}^{(l)}(0)|}\right)dt'$$
$$= -\frac{1}{\lambda_1}\left(\left\langle \ln\frac{|\mathbf{w}^{(l)}(t')|}{|\mathbf{w}(t')|}\right\rangle_t - \ln\frac{|\mathbf{w}^{(l)}(0)|}{|\mathbf{w}(0)|}\right).$$

One has

$$t\lambda_1(t) - t\lambda^{(l)}(t) = \zeta\sum_{r=1}^{N}[\tilde{\lambda}_1(t_r) - \tilde{\lambda}^{(l)}(t_r)]$$
$$\approx \zeta\sum_{r=1}^{\hat{t}_l/\zeta}[\tilde{\lambda}_1(t_r) - \tilde{\lambda}^{(l)}(t_r)].$$

The integrand in the definition of $\tau^{(l)}$ is therefore finite and usually different from zero when $t\to\infty$, which gives a $\tau^{(l)}$ different from zero. The latter may depend on the initial condition $\mathbf{w}(0)$; one has therefore to average the set $\{\tau^{(l)}\}$ over several different initial conditions. We have computed in [14] the set of $\tau^{(l)}$ for all DOFs, at various energies, and found negative and positive values. For large enough times, the expansion rate of the distance for initially close trajectories is λ_1; a negative (positive) time shift means that the corresponding DOF reaches a given level of expansion a time $\tau^{(l)}$ before (after) the whole system, i.e., the DOF is more chaotic (coherent) than the whole system. The dynamics of many condensed-matter systems, including the butane molecule, is determined by a Hamiltonian that can be approximated at low energy by a perturbed harmonic one. As this kind of Hamiltonian conveniently describes the Lennard-Jones crystal at low energy, the DOFs of those systems—in particular of the butane molecule—can be expected to have the kind of differentiated behavior found in Ref. [14].

In order to make a physically meaningful comparison among DOFs in different states of a system, or belonging to different systems, it is convenient to include the typical time after which the whole system manifests its chaoticity, i.e., the so-called Lyapunov time λ_1^{-1}. Therefore, we define the *coherence time* of a single DOF as $\bar{\tau}^{(l)}=\lambda_1^{-1}+\tau^{(l)}$. It can be seen as the time scale over which the single DOF is able to keep its coherence; it is a physical measure of the time needed by the single DOF to exhibit a chaotic behavior. Actually, a better measure of the degree of chaos of the whole system would be given by the sum of all positive Lyapunov exponents of its spectrum, $\Sigma_i^{(+)}\lambda_i$ (this sum corresponds to the Kolmogorov-Sinai entropy) [15]. We will show in Sec. V that—for the simulations reported in the present work—adding to λ_1 all other positive Lyapunov exponents and taking the inverse of this sum as a measure of the molecule's characteristic coherence time, the results do not change significantly. Therefore, we keep for simplicity the definition given above of coherence time for a single DOF. The coherence time of a DOF defines the degree of chaos or order characterizing its dynamics and is the combined effect of its proximity to the expanding and contracting directions in the phase space; but the measure of $\bar{\tau}^{(l)}$ does not require the previous determination of those directions. Therefore, the coherence times do not depend on the choice of the vectors used to compute the spectrum of Lyapunov exponents, the set of orthonormal vectors found in the usual Gram-Schmidt procedure (which we have used to find the results reported in Sec. V), or the set of Lyapunov covalent vectors determined through the procedure described in [16].

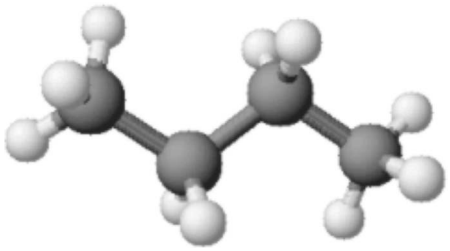

FIG. 1. Model of the butane molecule in the *trans*-conformation.

IV. BUTANE MOLECULE

We have used a united atom model to represent the butane molecule (C_4H_{10}) shown in Fig. 1: the hydrogen atoms are incorporated in the carbon atoms, giving four equally dressed point masses m [17,18]. As the mass of the molecule equals 58 amu, each mass point is endowed with a mass of 14.5 amu$=24.08\times10^{-24}$ g. In this model the potential energy is the sum of three terms: the vibrational energy of the covalent bonds (stretching), the vibrational energy of the valence angles (bending), and the energy associated with the dihedral torsion. If $\mathbf{r}_i=\{r_{i\alpha}\}(\alpha=x,y,z)$ are the Cartesian coordinates of the ith atom, the stretching is the variation in $\mathbf{b}_i=\mathbf{r}_{i+1}-\mathbf{r}_i(i=1,2,3)$. The bending is the variation in θ_i, where $\cos\theta_i=-\mathbf{b}_i\cdot\mathbf{b}_{i+1}/b_ib_{i+1}$.

The stretching energy is represented by a harmonic term: $V_s=\frac{1}{2}\Sigma_i\kappa_1(b_i-b_0)^2$; b_0 and b_i are the equilibrium distance and the actual distance between atoms i and $i+1$, respectively. The bending energy is represented by a sum of quadratic terms of the cosine of the valence angles θ: $V_b=\Sigma_i\kappa_2(\cos\theta_i-\cos\theta_0)^2$; θ_0 and θ_i are, respectively, the equilibrium angle and the actual angle between atoms i, $i+1$, and $i+2$ $(i=1,2)$. Let $\boldsymbol{\xi}_1$ and $\boldsymbol{\xi}_2$ be the normals to the planes defined by atoms 1,2,3 and 2,3,4, respectively: $\boldsymbol{\xi}_1=\mathbf{b}_1\times\mathbf{b}_2$, $\boldsymbol{\xi}_2=\mathbf{b}_2\times\mathbf{b}_3$; the dihedral angle is defined by $\cos\gamma=-(\boldsymbol{\xi}_1/|\boldsymbol{\xi}_1|)\cdot(\boldsymbol{\xi}_2/|\boldsymbol{\xi}_2|)$. The potential energy entailed in the dihedral angle γ is represented as $V_d=\Sigma_{j=0}^5 a_j\cos^j\gamma$ [19].

V_d has an absolute minimum at $\gamma=0$, $V_d=0$ (*trans*-conformation), and two relative minima symmetrically located at $\gamma=2\pi/3$, $V_d=2.926$ kJ/mol, as shown in Fig. 2. This energy corresponds to the *cis*-conformation. The torsion potential has two relative maxima at $\gamma=\pm\pi/3$, where it reaches the value $V_d=12.33$ kJ/mol, equivalent to a transition temperature above 124 K.

The total force acting on each mass point i has been computed by $\mathbf{f}_i=-\nabla_i(V_s+V_b+V_d)$, and the time evolution of the system has been simulated by molecular dynamics.

The computation of the explicit form of the forces in Cartesian coordinates is quite cumbersome; we report here the

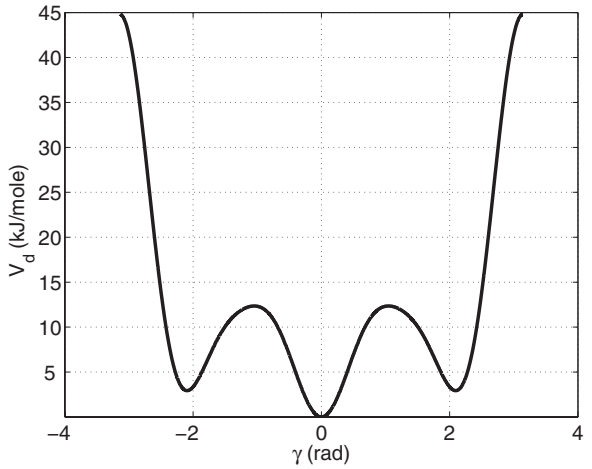

FIG. 2. Torsion potential of the dihedral angle in the range $[-\pi,\pi]$.

final results. Let $\mathbf{r}_i=\{r_{i,\alpha},\alpha=x,y,z\}$ be the position of the ith atom, and $\mathbf{b}_i=\mathbf{r}_{i+1}-\mathbf{r}_i$ $(i=1,2,3)$. We define

$$A_{i\alpha}\equiv-\frac{\partial V_s}{\partial r_{i\alpha}}=\kappa_1(b_i-b_0)\frac{r_{(i+1)\alpha}-r_{i\alpha}}{b_i}.$$

The forces acting on the four atoms derived from the stretching potential V_s have components $F_{1\alpha}=A_{1\alpha}$, $F_{2\alpha}=-A_{1\alpha}+A_{2\alpha}$, $F_{3\alpha}=-A_{2\alpha}+A_{3\alpha}$, and $F_{4\alpha}=-A_{4\alpha}$. For the forces deriving from the bending potential V_b we define

$$B_{i\alpha}\equiv\frac{\partial\cos\theta_i}{\partial r_{i\alpha}}=\frac{1}{b_i}\left[\frac{r_{(i+2)\alpha}-r_{(i+1)\alpha}}{b_{i+1}}+\cos\theta_i\frac{r_{(i+1)\alpha}-r_{i\alpha}}{b_i}\right],$$

$$C_{i\alpha}\equiv\frac{\partial\cos\theta_i}{\partial r_{(i+1)\alpha}}=\frac{1}{b_{i+1}}\left[\frac{r_{(i+1)\alpha}-r_{(i)\alpha}}{b_i}+\cos\theta_i\frac{r_{(i+2)\alpha}-r_{(i+1)\alpha}}{b_{i+1}}\right],$$

$$D_i\equiv-\frac{\partial V_b}{\partial\cos\theta_i}=-\kappa_2(\cos\theta_i-\cos\theta_0).$$

These forces then have components $F_{1\alpha}=D_1B_{1\alpha}$, $F_{2\alpha}=D_1(-B_{1\alpha}+C_{1\alpha})+D_2B_{2\alpha}$, $F_{3\alpha}=-D_1C_{1\alpha}+D_2(-B_{2\alpha}+C_{2\alpha})$, and $F_{4\alpha}=-D_2C_{2\alpha}$. In order to compute the torsional forces we define two vectors:

$$\mathbf{u}=\frac{1}{\xi_2}\left[\left(\frac{\boldsymbol{\xi}_1}{\xi_1}\right)+\left(\frac{\boldsymbol{\xi}_2}{\xi_2}\right)\cos\gamma\right],$$

$$\mathbf{v}=\frac{1}{\xi_1}\left[\left(\frac{\boldsymbol{\xi}_2}{\xi_2}\right)+\left(\frac{\boldsymbol{\xi}_1}{\xi_1}\right)\cos\gamma\right].$$

Defining

$$R\equiv\frac{\partial V_d}{\partial\cos\gamma}=\sum_{i=1}^{5}ia_i\cos^{i-1}\gamma,$$

the torsional forces on the four atoms are $\mathbf{F}_1=-R(\mathbf{b}_2\times\mathbf{v})$, $\mathbf{F}_2=R[(\mathbf{b}_1+\mathbf{b}_2)\times\mathbf{v}-\mathbf{b}_3\times\mathbf{u}]$, $\mathbf{F}_3=R[-\mathbf{b}_1\times\mathbf{v}+(\mathbf{b}_2+\mathbf{b}_3)\times\mathbf{u}]$, and $\mathbf{F}_4=-R(\mathbf{b}_2\times\mathbf{u})$.

We have performed a classical molecular dynamics simulation of a single butane molecule. Most of the results were obtained at constant total energy. The dynamics at constant energy has been obtained using the standard Verlet algorithm [20] to integrate the equations of motion. As we were interested in measuring and analyzing quantities related to the chaotic or coherent behavior of the DOFs of the system, we have chosen to avoid introducing unnecessary external constraints, which are likely to influence and modify these properties [21]. Therefore, we have not constrained the total energy, the total momentum, or the total angular momentum to a given value. The accurate numerical integration of the equations of motion maintained those quantities at their initial value, which was zero for the total momentum; the total angular momentum was zero in the simulations used to study the behavior of the internal variables (Sec. VI).

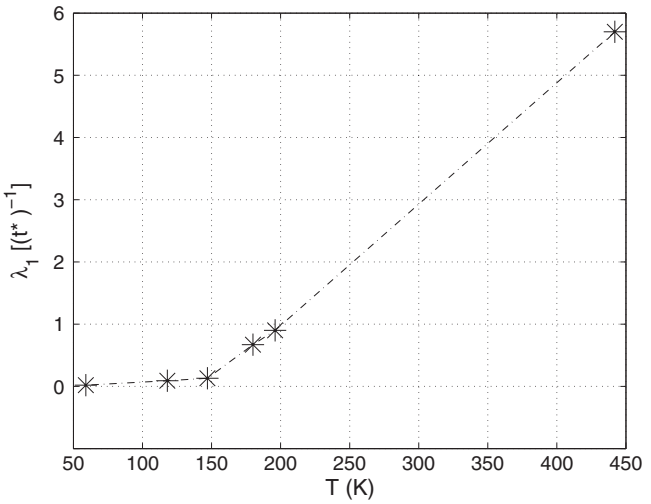

FIG. 3. Maximum Lyapunov exponent λ_1 as a function of the system's equilibrium temperature.

We have used a time step $h=0.21$ fs, which is 1/100 of the period T_s of the fastest vibration in the system, the stretching: $T_s=2.12\times10^{-2}$ ps. The precision of the Verlet algorithm is of $O(h^4)$ in the positions and of $O(h^2)$ in the velocities, and in a simulation at constant energy it allows an energy conservation within 0.01%; moreover, it has the advantage of being symplectic [22]. The duration of each simulated dynamics was about 100 ns; the length ζ of the short segments of the trajectory mentioned in Sec. III was 30 time steps. The temperatures simulated ranged from 54 to 442 K; in this range the dihedral angle can undergo transitions between the *trans*- and the *cis*-conformations. We have used in the following reduced units for length (σ^*) and time (t^*) [23] if not otherwise specified.

V. LYAPUNOV EXPONENTS

In order to estimate the degree of chaos of the butane molecule, we have computed the maximum Lyapunov exponent λ_1 at various total energies, corresponding to temperatures ranging from 54 to 442 K. The lowest temperature is below the energy threshold for the transition of the dihedral angle between potential wells and can be seen to produce only narrow oscillations inside the deepest potential well; the highest temperature is definitely above this threshold. In Fig.

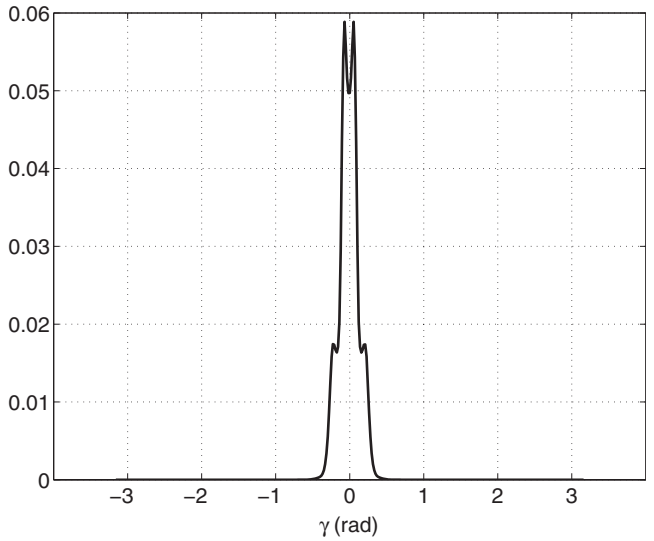

FIG. 4. Distribution of the dihedral angle at $T=147$ K; the area under the curve is normalized to 1 in this and in the two following figures.

3 we report the values of λ_1; as expected, the λ_1 values increase with temperature.

The sharp increase in the slope of λ_1 vs T between $T\sim 150$ K and $T\sim 180$ K can be related to the onset of the transition between wells of the dihedral potential, which are not-so-frequent and rapid events, as shown in Figs. 4–6.

The time given by the inverse of the maximum Lyapunov exponent is reported in Table I for each temperature; this Lyapunov time is assumed to represent a molecule's characteristic time for the loss of memory of its initial state, that is, for the display of a chaotic behavior. This time varies between $50t^*$ (97 ps) at the lowest temperature and $0.18t^*$ (0.35 ps) at the highest, showing how the onset of conformational transitions shortens the system's memory. The range of values of λ_1 between the lowest and the highest temperatures reflects the effect of the Hamiltonian's anharmonicity in a more striking way than the deviation from equipartition of

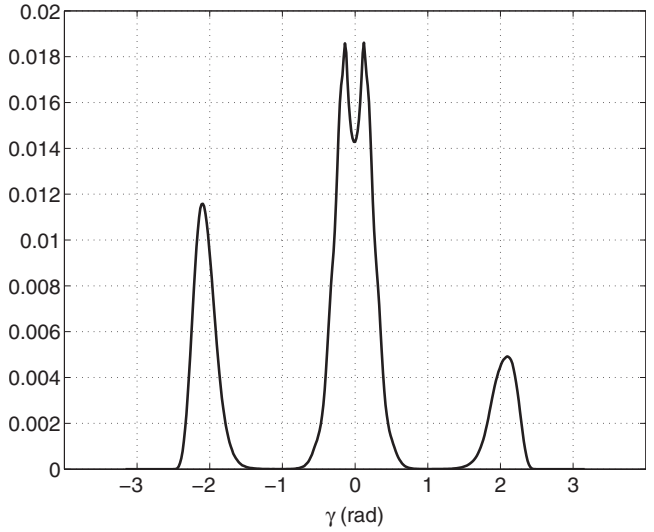

FIG. 5. Distribution of the dihedral angle at $T=180$ K.

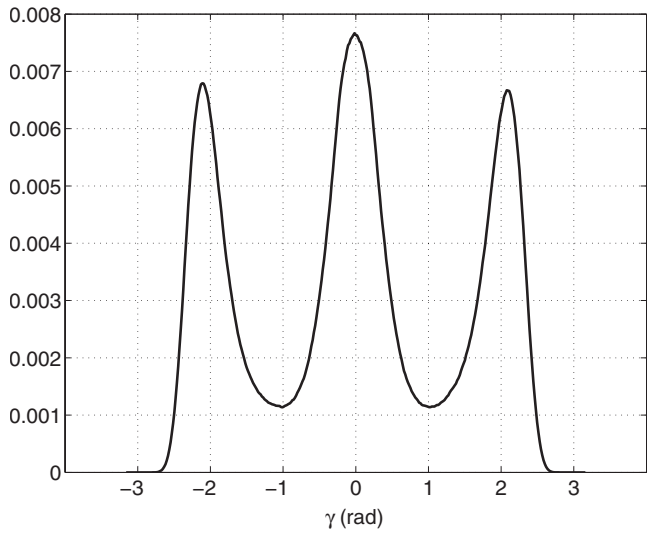

FIG. 6. Distribution of the dihedral angle at $T=442$ K.

energy; as a matter of fact, the latter—measured by $\eta=(\langle K\rangle-\langle U\rangle)/(\langle K\rangle+\langle U\rangle)$—increases only from 0.0894 at $T=59$ K to 0.0929 at $T=442$ K. Here $\langle K\rangle$ and $\langle U\rangle$ are the time averaged kinetic and potential energies, respectively.

We have measured the whole Lyapunov spectrum of the butane molecule at the three highest temperatures given in Table I, where the contribution of the Lyapunov exponents following the maximum is expected to be more significant. The results show the typical symmetrical structure of the Lyapunov spectrum above and below the zero value due to the symplectic property of the Hamiltonian. We have checked at these temperatures the sum rule $\Sigma_{i=1}^{24}\lambda_i=0$, where the sum extends over all Lyapunov exponents, and found it verified within 4×10^{-3} at $T=180$ K and 8×10^{-3} at $T=442$ K. If we add to λ_1 all other positive Lyapunov exponents and take the inverse of this sum as a measure of the molecule's characteristic coherence time, the results given in Table I for the Lyapunov times do not change significantly: $(\Sigma_i^{(+)}\lambda_i)^{-1}$ are (in reduced units) 1.4 at $T=180$ K, 0.47 at $T=196$ K, and 0.11 at $T=442$ K.

VI. COHERENCE TIMES OF THE INTERNAL VARIABLES

We performed simulations aimed at measuring the degree of coherence of the internal DOFs of the molecule: stretch-

TABLE I. Anharmonicity, λ_1, and Lyapunov time of the molecule at various temperatures T. λ_1 and λ_1^{-1} are in reduced units.

T (K)	η (%)	λ_1	λ_1^{-1}
59	8.94	0.02	50
118	9.01	0.09	11
147	9.04	0.13	7.7
180	9.06	0.67	1.5
196	9.08	0.9	1.1
442	9.29	5.7	0.18

TABLE II. λ_1^{-1} and all coherence times are given in reduced units. $\tilde{\tau}_c$ is the coherence time relative to each DOF; $\tilde{\tau}_v$ is the coherence time relative to its velocity. The total energy of the molecule is constant.

	$T=54$ K $\lambda_1^{-1}=222$		$T=168$ K $\lambda_1^{-1}=0.38$		$T=250$ K $\lambda_1^{-1}=0.26$	
	$\tilde{\tau}_c^{(l)}$	$\tilde{\tau}_v^{(l)}$	$\tilde{\tau}_c^{(l)}$	$\tilde{\tau}_v^{(l)}$	$\tilde{\tau}_c^{(l)}$	$\tilde{\tau}_v^{(l)}$
$\cos\theta_1$	1974	194	1.01	5.69	0	0
$\cos\theta_2$	1716	20	0.98	4.85	0.02	0.08
b_1	827	581	3.52	1.90	0	0
b_2	0	0	0.45	1.88	0.45	0.65
b_3	644	520	4.26	2.51	0	0
γ	361	515	0	3.46	0.02	0

ings, bendings, and the dihedral angle. These simulations were at constant total energy, with temperatures $T=54$, 168, and 250 K, given by the time average of the kinetic energy; the total momentum and the total angular momentum were initially equal to zero, and the integration of the equations of motion conserved those quantities. We report in Table II the coherence times $\tilde{\tau}_c^{(l)}$ of the six internal coordinates and the coherence times $\tilde{\tau}_v^{(l)}$ of their velocities; each value is an average over four trajectories with different initial conditions in the tangent space. At the lowest temperature ($T=54$ K), the maximum Lyapunov exponent is $\lambda_1=4.5\times10^{-3}$, which corresponds to a characteristic Lyapunov time of the molecule of $222t^*$, equivalent to 425 ps. The central stretching turns out to be the most chaotic DOF; actually it entails most of the chaotic behavior of the whole system, being the only one to have a coherence time shorter than the Lyapunov time of the molecule. As a matter of fact, its time shift ($-1970t^*$) is huge and means an instantaneous onset of a chaotic behavior; this appears in Table II as a zero coherence time. The other DOFs exhibit a clear coherence hierarchy, the bending angles being the most coherent ones, followed by the two external stretchings and the dihedral angle. The central stretching is also the most chaotic in the velocities subspace, while the bendings loose here their coherence, being more chaotic than the whole molecule. The most coherent DOFs in this subspace are the two external stretchings and the dihedral angle, as reported in Table II.

At the intermediate temperature ($T=168$ K) the dihedral angle undergoes transitions between potential wells. The onset of these transitions raises the value of λ_1 by 3 orders of magnitude to 2.6, which corresponds to a characteristic Lyapunov time of $0.38t^*$, equivalent to 0.74 ps; this dramatically shortens the coherence times, which now fall in the range of few picoseconds. The change in the dynamics of the dihedral angle is reflected in its coherence time, which turns out to be zero (actually corresponding to a negative time shift of $-3.1t^*$ in the coordinates' subspace), the lowest of all internal coordinates. As for the other coordinates, the external stretchings are now the most coherent, followed by the bendings; the central stretching is the least coherent. On the other hand, at this temperature, also the coherence times of the velocities display a hierarchy but a different one: the bendings are the most coherent, followed by the dihedral angle and by the stretchings.

At the highest temperature ($T=250$ K) the maximum Lyapunov exponent is $\lambda_1=3.8$, which corresponds to a characteristic time of $0.26t^*$, equivalent to about 0.5 ps. The further decrease in the coherence time is related to the intensification of transitions of the dihedral angle between neighboring potential wells, as shown in Figs. 4–6. At this high temperature the coherence times of almost all coordinates and velocities are in a narrow range near zero, with no significant distinction among them; the only exception is the central stretching, which turns out to be more coherent than all other DOFs at this high temperature.

The values λ_1 given in this section for the two highest temperatures—from which the molecule's Lyapunov times given in Table II are derived—are larger than the values that can be derived from the graph of Fig. 3 at the respective temperatures. The former have been computed in a simulation with zero total angular momentum of the molecule, while the latter have been computed with a total angular momentum that was constant but different from zero. The fraction of kinetic energy absorbed by the rotation was between 0.15 and 0.20, thus lowering the amount of kinetic energy effective in dynamically changing the shape of the molecule. If one translates this lower effective kinetic energy in a lower effective temperature, the two sets of λ_1 values become more similar. So, for example, the temperature at which the transitions of the dihedral angles set in—when the angular momentum is zero—turns out to be 120 K; this temperature practically coincides with the one found for this dynamical transition in the rotating molecule (147 K, as shown in Fig. 3), taking into account the fraction (0.16) of rotational kinetic energy in the latter case. Nevertheless, differences between the two sets remain after the correction of the nominal temperature of the rotating molecule. This point is discussed further in Sec. IX.

VII. PRINCIPAL COMPONENT ANALYSIS

We analyzed the dynamics of the butane molecule through the set of collective variables defined by means of the linear transformation of the vector $\mathbf{r}$ into $\mathbf{q}=O^T(\mathbf{r}-\langle\mathbf{r}\rangle)$, where O is the matrix the columns of which are the eigenvectors of the covariance matrix $C_\mathbf{r}=\langle(\mathbf{r}-\langle\mathbf{r}\rangle)(\mathbf{r}-\langle\mathbf{r}\rangle)^T\rangle$; $\langle\cdot\rangle$ is a time average. $O^TC_\mathbf{r}O$ is a diagonal matrix, the elements of which are the eigenvalues corresponding to those eigenvectors. The time evolution of vector $\mathbf{q}$ displays the essential dynamics of the molecule: it has been shown in the simulation of proteins that the components of $\mathbf{q}$ along few eigenvectors, corresponding to the largest eigenvalues of $C_\mathbf{r}$, account for most of the total fluctuation [24,25].

The same matrix O can be used to compute the velocities associated with $\mathbf{q}$ through the transformation $\dot{\mathbf{r}}=\{\dot{\mathbf{r}}_i\}$ into $\dot{\mathbf{q}}=O^T\dot{\mathbf{r}}$. We made a different choice, namely, we analyzed the velocity component of the dynamics by computing a covariance matrix for the velocities subspace: $C_\mathbf{v}=\langle(\mathbf{v}-\langle\mathbf{v}\rangle)(\mathbf{v}-\langle\mathbf{v}\rangle)^T\rangle$; we then projected the time evolution of the Cartesian velocities on the eigenvectors of this matrix, obtaining thus the collective momenta $\boldsymbol{\pi}$ (in this molecule all atoms

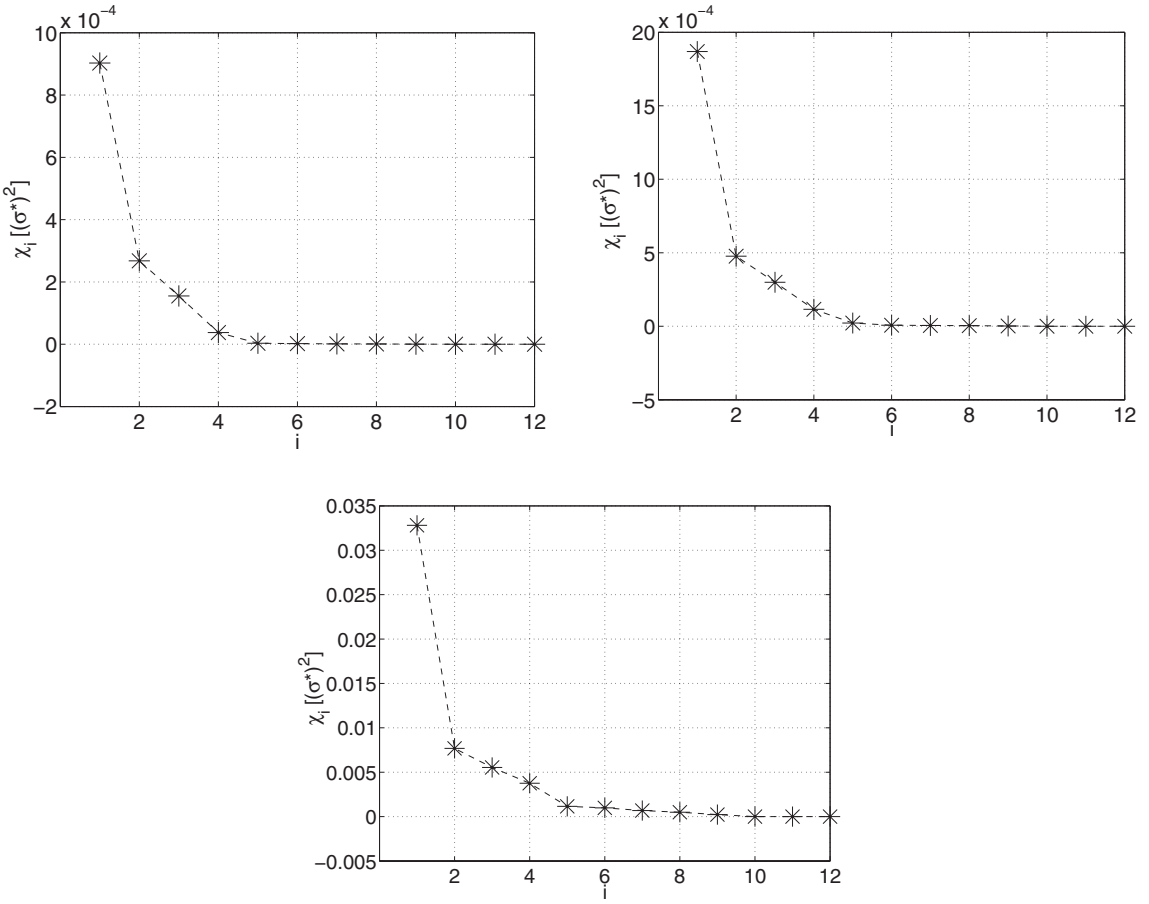

FIG. 7. Eigenvalues χ_i of the coordinates' covariance matrix $C_{\mathbf{r}}$.

have the same mass; therefore, the collective momenta are simply proportional to the collective velocities). The set of the so-called "essential" variables $\mathbf{q}$, $\boldsymbol{\pi}$ projects the dynamic evolution of the system onto a frame of reference suitable for evidencing a possible hierarchy in the amplitude of their fluctuations.

We report in Fig. 7 the eigenvalues χ_i of the positions' covariance matrix at temperatures $T=54$, 107, and 394 K, and in Fig. 8 the eigenvalues χ_i of the velocities' covariance matrix at the same temperatures. A nonzero angular momentum, albeit small, would produce rotations of the whole molecule giving to the atomic coordinates a fluctuation which would overshadow the amplitude of their variation in the frame of reference of the molecule; therefore, we performed these simulations by setting the total angular momentum to zero (these simulations were not used to compute the coherence times). The eigenvalues of the positions' covariance matrix show a sharp increase at the highest temperature, parallel to the one already observed in Fig. 3; as mentioned before, this increase is due to the activation of the transitions of the dihedral angle between nearby potential wells. Another relevant feature of these eigenvalues is that, at all simulated temperatures, the first eigenvalue is significantly larger (by a factor of about 4) than the following ones. As for the velocities' covariance matrix, at the two temperatures below the transition region the eigenvalues are split in two groups: the three highest eigenvalues are much larger (by a factor larger than 5) than the others; on the other hand at the highest temperature, where the dihedral angle undergoes transitions, the eigenvalues show a gradual decrease, without the gap present at the lower temperatures. Figures 7 and 8 show that even for a small molecule such as butane the PCA is able to extract the essential variables, both in the collective coordinates' and in the collective velocities' subspaces. With the exception of the velocities at the highest temperature, more than 90% of the total fluctuation of the molecule's positions and velocities is entailed in the first few variables. This result is similar to what is usually found in large biomolecules, for which the essential dynamics method was originally developed.

VIII. COHERENCE TIMES OF THE PRINCIPAL COMPONENTS

We have analyzed the behavior of subspaces $q^{(l)}$ or $\pi^{(l)}$, to which we associate subspaces $\delta q^{(l)}$ and $\delta\pi^{(l)}$ in the tangent space. We have looked for a possible correspondence between the amplitude of the eigenvalues of these two covariance matrices and the coherence in the corresponding essential subspaces. To this purpose, we have computed the following quantities.

$\lambda_1^{\mathbf{q}}(t)$, the estimated maximum Lyapunov exponent of the 12-dimensional (12D) subspace spanned by the set $\{q^{(l)}\}$,

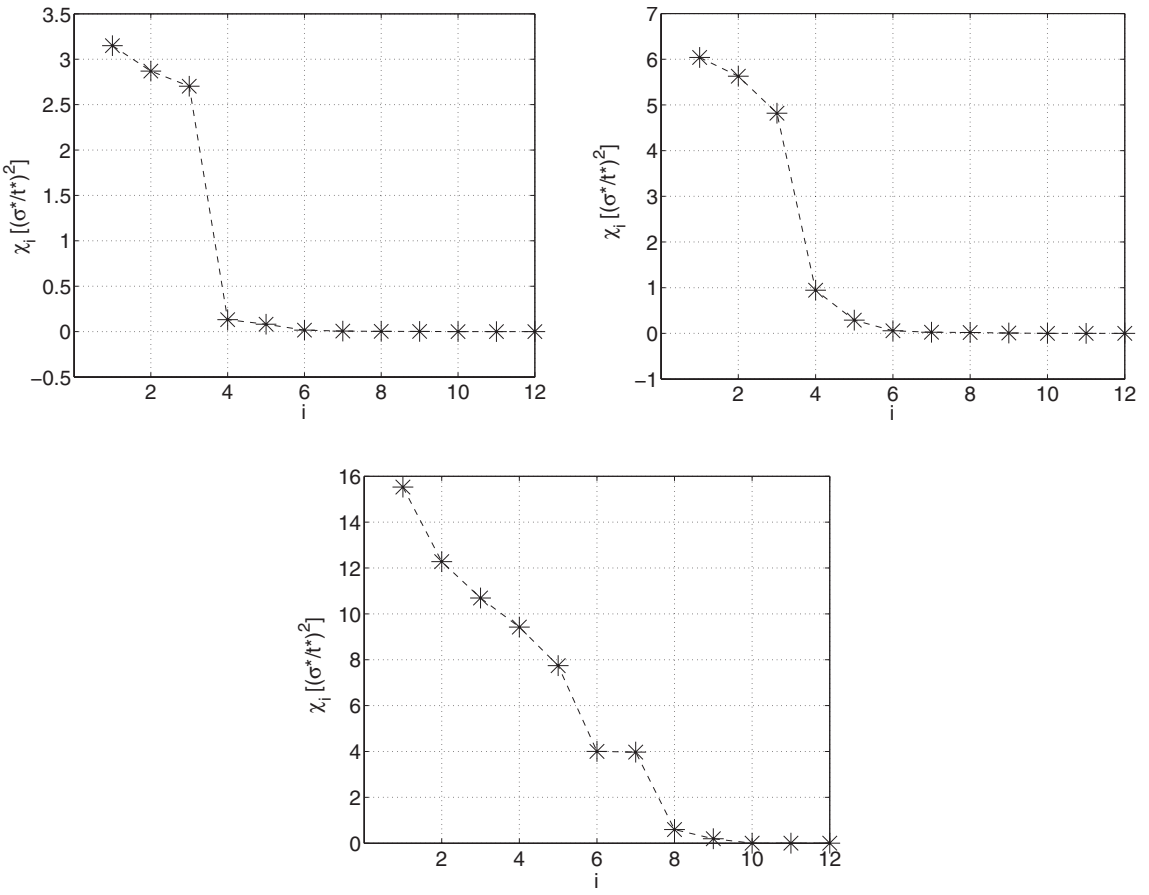

FIG. 8. Eigenvalues χ_i of the velocities' covariance matrix $C_{\mathbf{v}}$.

$$\lambda_1^{\mathbf{q}}(t) = \lim_{|\delta\mathbf{q}(0)|\to 0} \frac{1}{t} \ln \frac{|\delta\mathbf{q}(t)|}{|\delta\mathbf{q}(0)|}.$$

In analogous way we have computed $\lambda_1^{\boldsymbol{\pi}}(t)$, the estimated maximum Lyapunov exponent of the 12D subspace spanned by the set $\{\boldsymbol{\pi}^{(l)}\}$,

$$\lambda_1^{\boldsymbol{\pi}}(t) = \lim_{|\delta\boldsymbol{\pi}(0)|\to 0} \frac{1}{t} \ln \frac{|\delta\boldsymbol{\pi}(t)|}{|\delta\boldsymbol{\pi}(0)|}.$$

Asymptotically one has $\lim_{t\to\infty} \lambda_1^{\mathbf{q}}(t) = \lambda_1$ and $\lim_{t\to\infty} \lambda_1^{\boldsymbol{\pi}}(t) = \lambda_1$, where λ_1 is the maximum Lyapunov exponent of the whole system (because of topological invariance, this exponent may be equally computed in the Cartesian or in the essential space). We have verified these equalities as a check that the length of our simulation was sufficient to reach asymptotic values for the Lyapunov exponents.

The PLEs, which characterize the rate of divergence of the projection of two initially near trajectories on a single subspace, have been computed through

$$\lambda_q^{(l)}(t) = \lim_{|\delta q^{(l)}(0)|\to 0} \frac{1}{t} \ln \frac{|\delta q^{(l)}(t)|}{|\delta q^{(l)}(0)|}$$

and

$$\lambda_\pi^{(l)}(t) = \lim_{|\delta \pi^{(l)}(0)|\to 0} \frac{1}{t} \ln \frac{|\delta \pi^{(l)}(t)|}{|\delta \pi^{(l)}(0)|}.$$

Even though $\lim_{t\to\infty} \lambda_q^{(l)}(t) = \lim_{t\to\infty} \lambda_\pi^{(l)}(t) = \lambda_1 \, \forall \, l$, there are differences at finite times within each of the two sets $\{\lambda_q^{(l)}\}$ and $\{\lambda_\pi^{(l)}\}$. The compounded effect of these differences is just what generates the time shifts among the various DOFs, as explained in [14] and in Sec. III. Thus we compute the time shifts through

$$\tau_q^{(l)} = \frac{1}{\lambda_1} \lim_{t\to\infty} \frac{1}{t} \int_0^t t' [\lambda_1^{\mathbf{q}}(t') - \lambda_q^{(l)}(t')] dt',$$

$$\tau_\pi^{(l)} = \frac{1}{\lambda_1} \lim_{t\to\infty} \frac{1}{t} \int_0^t t' [\lambda_1^{\boldsymbol{\pi}}(t') - \lambda_\pi^{(l)}(t')] dt'.$$

As explained in Sec. III, the computation of the coherence times requires a measure of the PLEs relative to the various DOFs. As an example, we report in Figs. 9 and 10 the time evolution of selected PLEs, which show the kind of short time behavior that generates the different time shifts. In the first figure, relative to the positions subspace, the PLE relative to the ninth collective coordinate (corresponding to the ninth eigenvalue of the positions' covariance matrix) has a short time evolution which is below that of the whole positions' subsystem, hinting at a more coherent dynamics; on the other hand, the third collective coordinate has an opposite behavior, hinting at a more chaotic dynamics. For longer times both PLEs approach, as expected, the maximum Lyapunov exponent of the subsystem (which approaches as-

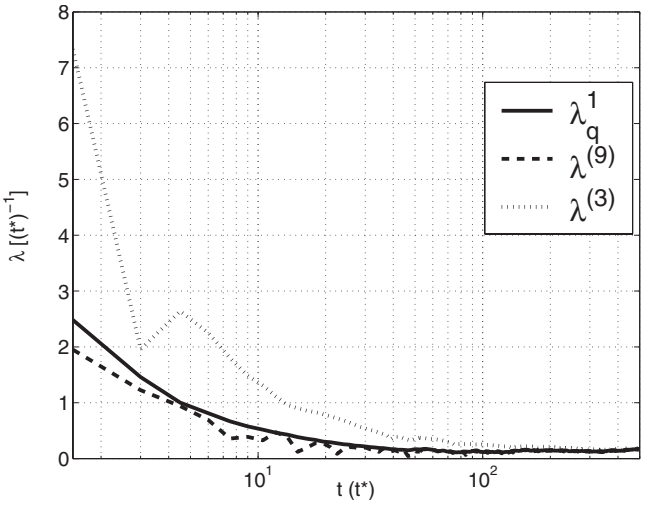

FIG. 9. Time evolution of two partial Lyapunov exponents and of $\lambda_1^{\mathbf{q}}(t)$ in the coordinates' subspace; $T=180$ K.

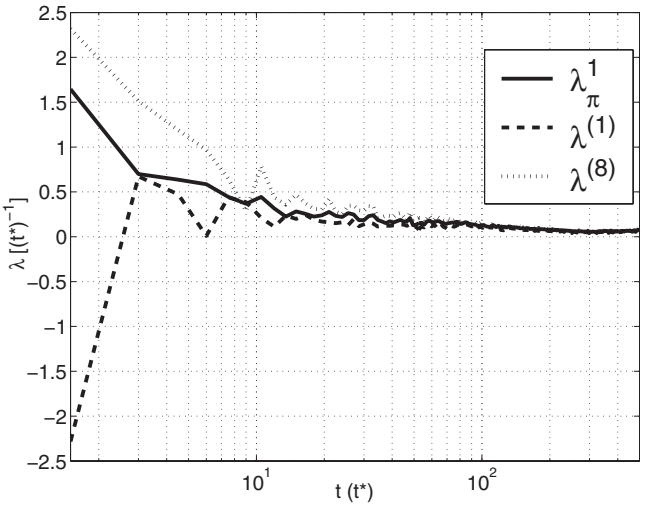

FIG. 10. Time evolution of two partial Lyapunov exponents and of $\lambda_1^{\boldsymbol{\pi}}(t)$ in the velocities' subspace; $T=147$ K.

ymptotically the maximum Lyapunov exponent of the whole system). These different behaviors are reflected in the different coherence times, as shown in Table III. In the second figure a similar difference is reported for the PLEs computed in the velocities' subspace. Here the eighth collective variable is more chaotic than the subsystem, while the first coordinate is more coherent; the coherence times relative to this subspace are also reported in Table III. It is interesting to note the different behavior of a given coordinate in the two subspaces, as an example, at $T=180$ K, the ninth collective coordinate is the second most coherent in the positions' subspace; but the same coordinate is among the most chaotic in the velocities' subspace. This is just an example of a rich variety of behaviors, which is reflected in a variety of coherence times, as shown in Table III.

All data reported in this table are taken from dynamical trajectories of length $5\times10^4 t^*$, which were long enough to produce stabilized values; each datum is an average over four trajectories with different initial conditions in the tangent space. All coherence times should be compared to λ_1^{-1} at the corresponding temperature; we take the latter, as mentioned before, as a measure of the coherence time of the whole molecule. Some regularities are evident: the first positional coordinate, corresponding to the maximum eigenvalue of the covariance matrix, is the most coherent DOF at the four highest simulated temperatures. A similar feature is more evident in the coherence times relative to the velocities' subspace, where the first variable is always the most coherent; moreover, at all temperatures but one ($T=180$ K), the second variable is also the second in coherence.

IX. DISCUSSION

The results of the present work show that some dynamical variables may need very long times (of the order of some ns) to display their chaotic behavior. In order to make use of the theoretical framework resumed in Sec. II, which applies to

TABLE III. Coherence times for the collective coordinates and velocities derived from a PCA at various temperatures. λ_1^{-1} and all coherence times are given in reduced units. The collective variables are listed in order of decreasing magnitude of the corresponding eigenvalue of the covariance matrix.

	$T=59$ K $\lambda_1^{-1}=50$		$T=118$ K $\lambda_1^{-1}=11$		$T=147$ K $\lambda_1^{-1}=7.7$		$T=180$ K $\lambda_1^{-1}=1.5$		$T=196$ K $\lambda_1^{-1}=1.1$		$T=442$ K $\lambda_1^{-1}=0.18$	
l	$\tilde{\tau}_q^{(l)}$	$\tilde{\tau}_\pi^{(l)}$	$\tilde{\tau}_q^{(l)}$	$\tilde{\tau}_\pi^{(l)}$	$\tilde{\tau}_q^{(l)}$	$\tilde{\tau}_\pi^{(l)}$	$\tilde{\tau}_q^{(l)}$	$\tilde{\tau}_\pi^{(l)}$	$\tilde{\tau}_q^{(l)}$	$\tilde{\tau}_\pi^{(l)}$	$\tilde{\tau}_q^{(l)}$	$\tilde{\tau}_\pi^{(l)}$
1	88	224	18	39	20	28	3.5	4.6	2.4	3.0	0.3	0.3
2	120	156	22	29	14	15	2.7	1.6	1.7	2.6	0.2	0.4
3	0	46	5	7	2.1	14	1.1	2.6	0.8	1.2	0.2	0
4	59	80	0	23	3.1	7.2	2.0	2.3	1.5	2.2	0.3	0.1
5	11	30	10	0	8.3	2.1	0	1.6	0.8	0.5	0.1	0
6	24	69	11	0	16	0	2.7	0	1.4	0	0.2	0.2
7	97	8	25	4	11	3.6	1.2	0.3	0.9	0	0.1	0.3
8	146	9	28	0	15	0	1.9	0	1.9	0	0.1	0.1
9	119	59	33	9	12	5.7	2.7	0	1.2	0	0.2	0.2

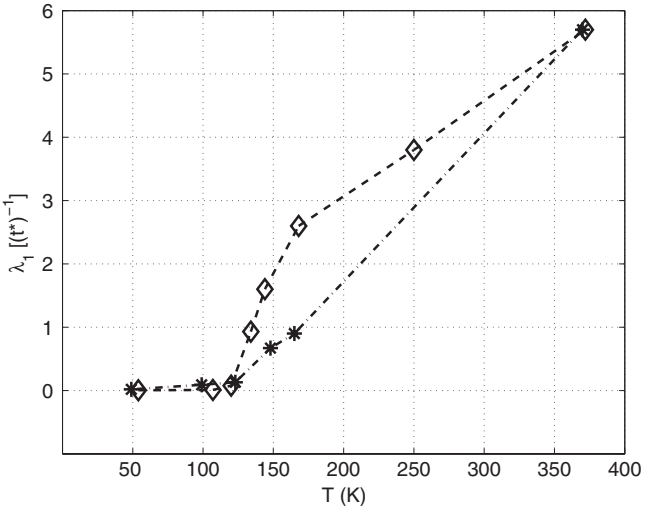

FIG. 11. Maximum Lyapunov exponent λ_1 as a function of the system's temperature corresponding to the internal kinetic energy. * rotating molecule; ◇ nonrotating molecule.

ergodic systems, we had to make sure that our simulations were long enough to allow all relevant dynamical variables to relax to equilibrium. This has been achieved by extending each of our simulations to about 100 ns, which is 25 times longer than the largest coherence time found in our computer experiments.

We distinguished the various simulations performed at constant total energy by their temperature. We could have rather used the time averaged total kinetic energy $\langle K \rangle$, as a thermodynamic parameter such as the temperature has limited meaning for a small isolated system such as the butane molecule. Nevertheless, we chose the temperature as it gives a more intuitive characterization of the physical state of a real system. But the relation between kinetic energy and temperature, as noticed at the end of Sec. VI, must be considered with care when dealing with a small system such as the butane molecule. The rotation of the molecule affects its dynamical regime, and the interplay of rotational and internal translational kinetic energy is not simple.

In Fig. 11 we report λ_1 for the rotating and the nonrotating (zero total angular momentum) molecules. In order to make a direct comparison of the two sets of data, the temperature of the rotating molecule has been computed—only for this figure—by averaging the internal kinetic energy, that is, the total kinetic energy minus the rotational kinetic energy. When the temperature of the rotating molecule is lowered by the amount corresponding to the rotational kinetic energy, the onset of the dihedral angle's transition takes place at similar temperatures (120–125 K) in both cases. But below and above that transition region the maximum Lyapunov exponent turns out to be different. At lower temperatures λ_1 is very small in both cases, but the rotating molecule exhibits a Lyapunov exponent that can be almost 1 order of magnitude higher (9.0×10^{-2} versus 9.3×10^{-3} in the 100–110 K region), hinting at a possible role of inertial forces (Coriolis and centrifugal) in enhancing chaos. On the other hand, at higher temperatures the nonrotating molecule produces a λ_1 that exceeds that of the rotating molecule in a broad temperature range. This difference diminishes for temperatures above 170 K and eventually vanishes around 370 K (all temperatures in this paragraph are internal). A comparison of the distributions of the dihedral angle near $T=170$ K, where the difference in λ_1 between the two cases reaches its maximum, shows that the nonrotating molecule spends a significant amount of time in the regions around $\gamma=\pm\pi/3$, where the potential has two relative maxima and the highest anharmonicity (see Fig. 2). On the other hand, the distribution of gamma for the rotating molecule is very similar to the one shown in Fig. 5, with almost no time spent in that highly anharmonic region. While the different dynamical behavior accounts for the different degree of chaos, the origin of this behavior deserves further investigation.

The coherence time $\tilde{\tau}^{(l)}$ qualifies the dynamical behavior of a degree of freedom and shows the time after which it becomes chaotic. This time is related to the angular distance of the tangent subspace corresponding to that DOF from all expanding directions foreseen by the Oseledec theorem, namely the directions characterized by positive Lyapunov exponents: the narrower the angular distance from the directions corresponding to the highest Lyapunov exponents, the shorter the coherence time. Some DOFs are characterized by a degree of chaos that exceeds that of the whole system, and—at all temperatures reported in this paper—the absolute value of their negative time shift may be larger than the Lyapunov time λ_1^{-1}. For these DOFs the coherence time would be negative; because of the physical content we attach to this parameter, its negative values have been replaced by zeros in Tables II and III, meaning an instantaneous onset of a chaotic behavior.

$\tilde{\tau}^{(l)}$ summarizes, in one single number, the effect of all generalized coherence angles introduced previously [11,12] to measure the coherence of a single DOF. In order to compute it correctly, one should add the time shift characteristic of the DOF to the time characterizing the coherence of the whole system, that is, the inverse of the Kolmogorov-Sinai entropy $\Sigma_i^{(+)}\lambda_i$, which takes into account the effect of all expanding directions in the phase space [15]. For simplicity, as mentioned at the end of Sec. III, we have summed instead the time shifts to the Lyapunov time λ_1^{-1}, as the computation of the whole Lyapunov spectrum at low temperature requires very long trajectories; this approximation does not change significantly the coherence times reported in Tables II and III. This has been checked at the highest temperatures, where the effect of the expanding directions other than the first one is expected to be more significant; on the other hand, at these temperatures, the whole Lyapunov spectrum can be computed on relatively short trajectories.

In a previous work done on a thermalized butane molecule, the coherence of the molecule's DOFs was measured by computing coherence angles and generalized coherence angles for the collective variables $x_i=(q_i,\pi_i)$, $i=1,\ldots,9$, defined through the essential variables introduced in Sec. VII [12]. In order to compare the coherence times computed in this paper with the coherence angles reported in [12], we can observe that the latter are determined mainly by the least coherent variable in each pair (q_i,π_i), as this variable plays the major role in increasing the distance between the projections on the (q_i,π_i) plane of two initially near trajectories.

Therefore, a comparison can be done between the coherence angle of a DOF and the shortest between its coherence times $\tilde{\tau}_q^{(l)}$ and $\tilde{\tau}_\pi^{(l)}$. The data obtained at $T=140$ K in [12] can be compared with the data at $T=147$ K given in Table III. For the first four variables the coherence times to be compared with the coherence angles are the $\tilde{\tau}_q^{(l)}$, for the remaining variables the $\tilde{\tau}_\pi^{(l)}$. Notwithstanding the different conditions of the two simulations—the molecule is isolated here and thermalized in [12]—the two measures of coherence identify the same set of essential variables as the most coherent and in the same order. In Fig. 2 of Ref. [12] the largest coherence angles (corresponding to a higher coherence) are—in decreasing order—the first, the second, the fourth, and the third. This is the same hierarchy found in Table III at $T=147$ K, if one neglects the collective variables beyond the fourth [they correspond to eigenvalues of the coordinates' covariance matrix that are almost zero (see Fig. 7)]. The introduction of a thermal bath does not seem thus to alter significantly the overall qualitative pattern of the essential dynamics.

X. CONCLUSION

The computation of coherence times of collective variables, which was the main objective of this work, has been performed for two sets of collective variables, namely, the internal coordinates (stretchings, bendings, and dihedral angle) and the variables produced by a principal component analysis of the Cartesian coordinates (essential variables). The simulation has been done on a temperature range large enough to encompass distinct dynamical patterns of the molecule: from weakly chaotic to strongly chaotic. In the first low temperature regime all atoms move in the neighborhood of the bottom of a multidimensional potential well; in the second high temperature regime large spatial movements take place due to transitions of the dihedral angle between near potential wells.

A first result of our simulation is the sharp change in Lyapunov times as the temperature is raised above the region (between 150 and 170 K) where transitions of the dihedral angle start taking place. Below that transition the molecule as a whole is weakly chaotic, with a characteristic λ_1 varying between 0.02 and 0.13 for temperatures from 59 to 147 K (see Table I). These values of λ_1 correspond to Lyapunov times of the whole system varying between 97 and 15 ps. As soon as the conformational transitions begin, just above 150 K, the Lyapunov time drops abruptly below 3 ps, a clear sign of the increase in chaotic behavior.

A second result is the strong difference in coherence times between the two sets of collective variables below the transition region. The internal variables are characterized by coherence times that can reach thousands of picoseconds (see Table II) at the lowest simulated temperature, 1 order of magnitude higher than the essential variables at a similar temperature. This implies a warning regarding the use of computer experiments to measure statistical properties of molecules, as mentioned in Ref. [11]. In order to assume an equivalence between time averages performed during the computer experiment and ensemble averages, the time of the computer simulation should exceed by at least 1 order of magnitude the coherence time characterizing the most coherent DOF relevant to the experiment. Therefore, in planning a computer simulation to analyze low temperature properties of a molecule that depend on internal variables, one should be aware of the very long coherence times reported in Table III. This should hold also for macromolecules that entail hundreds or thousands of internal variables, as one would not expect the coherence times of stretchings and bendings to be very different from those found in the butane molecule. On the other hand, the dynamics of a dihedral angle in a macromolecule may have a different character than the one found in the present simulation, as its transitions would imply extended movements of large segments of the molecule.

A third result is the differences among variables of the same set and between coordinates and velocities. The internal DOFs exhibit below the transition region a clear hierarchy of coherence: looking at the coordinates subspace, the two bendings are the most coherent, followed by the external stretchings, then by the dihedral angle, and by the central stretching. Looking at the velocities subspace one also finds a clear coherence hierarchy but a different one: the two external stretchings are the most coherent, followed by the dihedral angle; the two bendings are more chaotic than the system, and the central stretching is the most chaotic of all also in this subspace. These large differences among DOFs reflect the prediction of Nekhoroshev's theorem [3], namely, that in a near integrable system different DOFs may exhibit a chaotic behavior on different time scales. As a matter of fact, at low temperature all internal DOFs are near the bottom of the respective potential well, and the molecule's dynamics is very regular. As soon as the temperature is raised above the transition region (see Table II, at $T=168$ K), the differences among the various coherence times become less relevant, even though the dihedral angle is now clearly the most chaotic in the coordinates subspace, and the two external stretchings are the most coherent; in the velocities subspace the two bendings are the most coherent, followed by the dihedral angle. The three stretchings are less coherent, but still more coherent than the whole system, the chaoticity of the latter being mainly determined by the behavior of the dihedral coordinate. At still higher temperature ($T=250$ K) all DOFs have become similarly chaotic, in both subspaces, with the exception of the central stretching, which is now the most coherent DOF.

The last result regards the collective variables derived from the principal component analysis. Here too one finds a significant reduction in the coherence times when the temperature is raised into and above the transition region of the dihedral angle. Looking in the coordinate subspace one does not see a clear distinction among them below the transition region. Once the transitions of the dihedral angle set in, the first coordinate (which is the projection on the eigenvector corresponding to the largest eigenvalue of the covariance matrix) becomes the most coherent in all cases. A clear distinction among variables is found in the velocities subspace: here the first two variables turn out to be more coherent than the remaining ones in the whole temperature range (with

only one exception for the second velocity). The difference is very significant at the lowest temperature (see Table III) and is present—albeit on a lesser level—even at temperatures above the transition region. This persistence of the largest fluctuations of the collective velocities seems to deserve further study, especially in larger molecules which may present a variety of extended conformational transitions.

ACKNOWLEDGMENTS

We thank Professor Harald Posch for providing us with the model of the butane molecule. We are also indebted to Dr. Lapo Casetti for his contribution to the simulation computer program. We also wish to thank Professor G. Gallavotti and Professor L. Galgani for useful discussions.

[1] E. Fermi, J. Pasta, and S. Ulam, Los Alamos Report No. LA-1940, 1955; later published by E. Fermi, *Collected Papers* (University of Chicago Press, Chicago, 1965).

[2] A. N. Kolmogorov, Dokl. Acad. Nauk SSSR **98**, 527 (1954); *Stochastic Behaviour in Classical and Quantum Hamiltonian Systems*, Lecture Notes in Physics Vol. 93, edited by G. Casati and G. Ford (Springer-Verlag, Berlin, 1979); J. Moser, Nachr. Akad. Wiss. Goett. II, Math.-Phys. Kl., pg. 1 (1962); V. I. Arnold, Usp. Mat. Nauk **18**, 13 (1963); Russ. Math. Surveys **18**, 9 (1963); Usp. Mat. Nauk **18**, 91 (1963); Russ. Math. Surveys **18**, 85 (1963).

[3] N. N. Nekhoroshev, Trans. Mosc. Math. Soc. **32**, 1 (1977).

[4] G. Benettin, G. Lo Vecchio, and A. Tenenbaum, Phys. Rev. A **22**, 1709 (1980).

[5] G. Benettin and A. Tenenbaum, Phys. Rev. A **28**, 3020 (1983).

[6] V. I. Oseledec, Trans. Mosc. Math. Soc. **19**, 197 (1968).

[7] G. Benettin, L. Galgani, and J. M. Strelcyn, Phys. Rev. A **14**, 2338 (1976).

[8] S. V. Ershov and A. B. Potapov, Physica D **118**, 167 (1998).

[9] G. Benettin, L. Galgani, A. Giorgilli, and J. M. Strelcyn, C. R. Seances Acad. Sci., Ser A **268**, 431 (1978).

[10] M. D'Alessandro and A. Tenenbaum, Phys. Rev. E **52**, R2141 (1995).

[11] M. D'Alessandro, A. D'Aquino, and A. Tenenbaum, Phys. Rev. E **62**, 4809 (2000).

[12] M. D'Alessandro, A. Tenenbaum, and A. Amadei, Phys. Rev. E **66**, 020901(R) (2002).

[13] I. Borzsák, H. A. Posch, and A. Baranyai, Phys. Rev. E **53**, 3694 (1996).

[14] M. D'Alessandro, A. D'Aquino, and A. Tenenbaum, Physica A **240**, 115 (1997).

[15] Y. B. Pesin, Russ. Math. Surveys **32**, 55 (1977).

[16] F. Ginelli, P. Poggi, A. Turchi, H. Chaté, R. Livi, and A. Politi, Phys. Rev. Lett. **99**, 130601 (2007).

[17] J. P. Ryckaert, I. R. McDonald, and M.-L. Klein, Mol. Phys. **67**, 957 (1989).

[18] S. Toxvaerd, J. Chem. Phys. **93**, 4290 (1990).

[19] $b_0=1.53$ Å, $k_1=350$ kJ/mol Å^2 [H. Posch (private communication)], $\theta_0=1.91$ rad, and $k_2=520$ kJ/mol [18]. $a_0=9.279$, $a_1=12.156$, $a_2=-13.120$, $a_3=-3.060$, $a_4=26.240$, and $a_5=-31.495$ kJ/mol [17].

[20] L. Verlet, Phys. Rev. **159**, 98 (1967).

[21] M. D'Alessandro, A. Tenenbaum, and A. Amadei, J. Phys. Chem. B **106**, 5050 (2002).

[22] L. Casetti, Phys. Scr. **51**, 29 (1995).

[23] Length $\sigma^*=3.923$ Å; energy $\epsilon^*=598.63/N_A$ J, where N_A is Avogadro's number; mass $m^*=14.5$ amu$=24.8\times10^{-27}$ kg; and time $t^*=\sigma^*\sqrt{m^*/\epsilon^*}=1.93$ ps.

[24] A. Amadei, A. B. M. Linssen, and H. J. C. Berendsen, Proteins **17**, 412 (1993).

[25] A. Amadei, B. L. de Groot, M. A. Ceruso, M. Paci, A. Di Nola, and H. J. C. Berendsen, Proteins **35**, 283 (1999).